Access from the University of Nottingham repository:

Copyright and reuse:

A note on versions:

Presence of Time-Dependent Diffusion in the Brachial Plexus

AQ1

AQ2 AQ6   Zaid B. Mahbub,[1,2] Andrew M. Peters,[2] and Penny A. Gowland[2]*

Purpose: This work describes the development of a method to measure the variation of apparent diffusion coefficient (ADC) with diffusion time (Δ) in the brachial plexus, as a potential method of probing microstructure.
Methods: Diffusion-weighted MRI with body signal suppression was used to highlight the nerves from surrounding tissues, and sequence parameters were optimized for sensitivity to change with diffusion time. A porous media-restricted diffusion model based on the Latour-Mitra equation was fitted to the diffusion time-dependent ADC data from the brachial plexus nerves and cord.
Results: The ADC was observed to reduce at long diffusion times, confirming that diffusion was restricted in the nerves and cord in healthy subjects. *T2* of the nerves was measured to be 80 ± 5 ms, the diffusion coefficient was found to vary from $(1.5 \pm 0.1) \times 10^{-3}$ mm^2/s at a diffusion time of 18.3 ms to $(1.0 \pm 0.2) \times 10^{-3}$ mm^2/s at a diffusion time of 81.3 ms.
Conclusion: A novel method of probing restricted diffusion in the brachial plexus was developed. Resulting parameters were comparable with values obtained previously on biological systems. **Magn Reson Med 000:000–000, 2017. © 2017 International Society for Magnetic Resonance in Medicine.**

Key words: brachial plexus; ADC; diffusion time; restricted diffusion

INTRODUCTION

The brachial plexus provides motor and sensory innervation to the upper extremities, and its function can be compromised in disorders such as cervical spondylosis, radiculopathy, and/or myelopathy. Quantitative MRI may provide a means of monitoring changes in tissues particularly during response to therapy. In particular, diffusion, and the effects of hindered or restricted diffusion, may provide information about changes in tissue microstructure.

MRI can be used to measure both the apparent diffusion coefficient (ADC), and the diffusion time (Δ) dependence of the ADC, which is an indicator of compartment size. At short diffusion time, most water molecules are unlikely to have diffused far enough to interact with the

boundaries, but at longer diffusion times the measured ADC will be reduced if molecular motion is restricted within, or hindered between, axons. In the brachial plexus, the diameter of the nerve fibers is the range between 5 and 15 μm (1,2) with smaller distances between them, so assuming a free water diffusion coefficient of $D = 2 \times 10^{-3}$ mm^2/s at body temperature (3), the molecular displacement would be hindered or restricted at times up to $\sim$50 ms, which overlaps the accessible range of diffusion times for a human MR scanner. Thus, it should be possible to use diffusion MRI to probe changes in the size or spacing of axons in the brachial plexus.

In order to allow comparison between subjects, it is useful to be able to parameterize the diffusion time dependence of the ADC. Various models have been used to do this, including the intra-axonal restricted and extra-axonal hindered diffusion (CHARMED) model (4,5), models considering cell membrane hindering (6), and models considering cell membrane permeability and density effects (7). Here, we have used the porous media model (8,9), which provides a simple, physically based method for parameterizing the diffusion time dependence of ADC ($D(\Delta)$), based on the Mitra equations (10–13). This model was initially proposed for use in biological tissues (14) and has been applied to various biological systems in vivo (15) and ex vivo (8,16,17) and to microstructure phantoms (18,19), but, as we are aware, it has never previously been used for in vivo human tissues. For restricted diffusion in porous media, Latour et al (14) simplified the model using a Pade approximant to Equation [1]:

$$D(\Delta) = Do\left\{1 - \left(1 - \frac{1}{\alpha}\right)\left(\frac{c\sqrt{\Delta} + \frac{(1-\frac{1}{\alpha})\Delta}{\theta}}{(1-\frac{1}{\alpha}) + c\sqrt{\Delta} + \frac{(1-\frac{1}{\alpha})\Delta}{\theta}}\right)\right\} \quad [1]$$

where D_o is the unrestricted self-diffusion coefficient, Δ is the diffusion time, $c = \frac{4}{9\sqrt{\pi}}\left(\frac{S}{V}\right)\sqrt{D_o}$, θ is a time scaling factor, which depends on the characteristic size of restricting and hindering microstructure, α is the (dimensionless) tortuosity index of the medium, relevant in the long Δ regime in which spins diffuse greater distances than the characteristic restriction lengths and hence sample the connectivity of spaces within the tissue, and S/V (mm^{-1}) is the surface-to-volume ratio of the medium reflected in the short Δ regime where surfaces are probed by a fraction of molecules.

MRI of the brachial plexus is technically challenging because of the size and location of the nerves, which can result in problems in identification, partial volume errors, distortion, and artefacts, but diffusion-weighted imaging (DWI) with background suppression (DWIBS)

[1]Department of Arts & Sciences, Ahsanullah University of Science & Technology, Dhaka, Bangladesh.
AQ3

[2]Sir Peter Mansfield Imaging Centre, School of Physics & Astronomy, University of Nottingham, United Kingdom.

*Correspondence to: Penny Gowland, SPMIC, School of Physics and Astronomy, University of Nottingham, NG7 2RD, United Kingdom. E-mail:
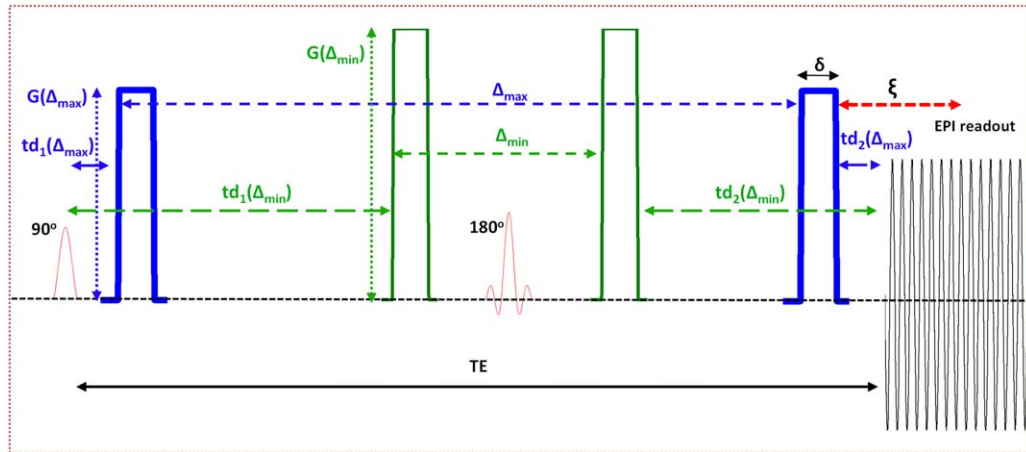AQ5   Penny.gowland@nottingham.ac.uk

1

Mahbub et al.

FIG. 1. DWIBS sequence with timing parameters. $TE = \Delta + td_1 + td_2 + \delta + \xi$ and it can be seen that variations in the delay times td_1, td_2, and gradient amplitudes G result in the required diffusion times Δ_{min} and Δ_{max} at fixed b-values. (Left to Right 1st part) $G(\Delta_{max})$ $G(\Delta_{min})$ Δ_{max} δ ξ, (Left to Right 2nd part) $td_1(\Delta_{max})$ Δ_{min} $td_2(\Delta_{max})$ EPI readout, (Left to Right 3rd part) 90° $td_1(\Delta_{min})$ 180° $td_2(\Delta_{min})$, (Bottom) TE.

(20,21) provides a method of isolating nerves from the other soft tissues (22). DWIBS uses inversion recovery to null the fat signal independent of frequency offset and *T2* and diffusion weighting to suppress surrounding tissues. The resulting images can be reconstructed as maximum intensity projections (MIPs) to illustrate the relative positions of the nerve roots and nerve paths. Several qualitative studies using DWIBS have shown that this technique has potential value in the assessment of pathological changes, including in the brachial plexus (22–26).

The aim of this work was to develop a robust method for measuring the diffusion time dependence of ADC ($D(\Delta)$) in the brachial plexus nerves and cord, and to parameterize the results using the porous media-restricted diffusion model.

METHODS

F1   A sequence was written to allow the diffusion time (Δ) to be varied for fixed b values (Fig. 1) and optimized to measure diffusion time-dependent changes in a diffusion coefficient. Initial experiments were performed to investigate any nondiffusive effects in the DWI signals from the brachial plexus (i.e., intravoxel incoherent motion [IVIM], taken to include any dephasing attributed to nondiffusive motion), and to determine the *T2* of the nerves (27,28). Finally, the sequence was used to assess $D(\Delta)$ in the brachial plexus.

Development of the Sequence

The sequence shown in Figure 1 (which defines timing parameters) was coded on a 3 T Philips Achieva scanner (Philips Medical Systems, Best, The Netherlands). The three gradient coils were driven simultaneously to produce the maximum achievable diffusion gradient, which was necessary to be able to vary diffusion time within a reasonable echo time (*TE*), particularly given that it would not be possible to vary both diffusion time and diffusion direction in a feasible scanning time. This provided diffusion encoding at 45° to the x-axis and 70⁰ to

the z-axis of the scanner, which is approximately perpendicular to the fibers of the brachial plexus as they curve around the neck.

The maximum achievable value of diffusion time Δ_{max} is limited by echo time ($TE = \Delta + td_1 + td_2 + \delta + \xi$), and for a given value of b the minimum diffusion time Δ_{min} is determined by the maximum achievable gradient amplitude. Table 1 shows the range of accessible values   T1 of Δ, determined by considering achievable values of gradient lobe length (δ), delay times (td_1 and td_2), and gradient amplitudes (G) for required values of b and *TE*, assuming the time between the end of the second gradient lobe and the center of k-space was $\xi = 19.7$ ms for the Philips Achieva 3T scanner used (Philips Medical Systems).

Optimization of Sequence Parameters

Within the constraints of the limited information available about the geometry and permeability of the nerve fibers, we attempted to maximize sensitivity to changes in ADC across the range of accessible diffusion times ($D(\Delta)$). For clinical imaging systems, long echo times are required to assess restricted or hindered diffusion, which reduces the signal-to-noise ratio (SNR) of the data and leads to a trade-off between contrast and sensitivity. Ideally, one would want to probe the variation in ADC across a wide range of diffusion times, but that is not

Table 1

Range of Achievable Diffusion Time Δ at Different b-values, for $\delta = 10$ ms and $TE = 100$ or 85 ms, on the 3T Philips Achieva Scanner.

b (s/mm²)	$TE = 100$ ms		$TE = 85$ ms	
	Δ_{min}	Δ_{max}	Δ_{min}	Δ_{max}
300	18.3	81.3	18.3	62.3
600	18.3	81.3	18.3	62.3
850	20.3	81.3	18.3	62.3
1,100	23.3	81.3	22.3	62.3
1,300	29.3	81.3	26.3	62.3
1,500	31.3	81.3	32.3	62.3

feasible in vivo, so instead we aimed to identify a range of diffusion times that would give a large change in ADC ~~that~~ could be detected with high sensitivity. First, we defined the diffusivity difference as a measure of the dynamic range of the experiment (maximum detectable change in diffusion coefficient with diffusion time) (Eq. [2]):

$$K(\Delta_{\min}, \Delta_{\max}) = D_1(\Delta_{\min}) - D_2(\Delta_{\max}) \qquad [2]$$

where D_1 is the ADC measured at short diffusion time ($\Delta_{\min}$) and D_2 is the ADC measured at long diffusion time ($\Delta_{\max}$). We then defined the contrast to noise in diffusivity difference as shown by Equation [3]:

$$\Gamma_K(\Delta_{\min}, \Delta_{\max}) = \frac{K(\Delta_{\min}, \Delta_{\max})}{\sigma_K} \qquad [3]$$

Ideally, we would sample diffusion at a range of b values and a range of diffusion times, but this is not feasible in vivo. It has previously been shown that for pure Brownian motion, the diffusion coefficient (D) is optimally measured at two b values (29–31) and we used these values as the best estimate for this initial work (Eq. [4]):

$$D = \frac{ln S_1 - ln S_2}{b_2 - b_1} \qquad [4]$$

where S_1 and S_2 are the signals at b_1 and b_2, respectively (Eq. [5]):

$$S_i = S_0 e^{(-b_i D)} e^{(-TE/T2)}, \quad i = 1, 2 \qquad [5]$$

By propagation of errors, the variance in the calculated value of D is given by Equation [6]:

$$\sigma_D^2 = \frac{\sigma_S^2}{(b_2 - b_1)^2} \frac{1}{\left(S_0 e^{-\frac{TE}{T2}}\right)^2} (e^{2b_1 D} + e^{2b_2 D}) \qquad [6]$$

(where σ_S is the variance of the noise in the raw images), which has a minimum σ_D for $b_2 D = 1.1$ (29,31).

The variance in K is given by Equation [7]:

$$\sigma_K = (\sigma_{D_1}^2 + \sigma_{D_2}^2)^{1/2} \qquad [7]$$

and substituting from Equation [6], this gives Equation [8]:

$$\sigma_K = \left[\frac{\sigma_S^2}{(b_2 - b_1)^2 \left(S_0(b_1)\right)^2 e^{-\frac{2TE}{T2}}} \left(2 + e^{2(b_2 - b_1)D_1} + e^{2(b_2 - b_1)D_2}\right) \right]^{1/2} \qquad [8]$$

This analysis neglects the effect of the Rician noise distribution, and, experimentally, data points below the noise floor were ~~removed~~ (see Methods). To estimate Γ_K, an estimate of the change in ADC with diffusion time is required. Therefore, a Monte Carlo simulation of diffusion restricted by impermeable boundaries with different restriction sizes (R) was used to estimate the change in ADC with Δ for different values of TE. It was assumed that $b_1 = 0$ and $b_2 = 50, 100, 150, 200, 250, 300, 400,$ and 500 s/mm², although if b_1 had to be greater than zero for

other reasons, then b_2 could be replaced by $(b_2 - b_1)$ and the final results scaled by $S_0(b_1)/S_0 0$. For R of 20 µm and 5 µm, the variation of Γ_K with b value was investigated for $TE = 85$ ms ($\Delta_{\min} = 18.3$, $\Delta_{\max} = 66.3$ ms), $TE = 100$ ms ($\Delta_{\min} = 18.3$ ms, $\Delta_{\max} = 81.3$ ms), and $TE = 110$ ms ($\Delta_{\min} = 18.3$ ms, $\Delta_{\max} = 91.3$ ms), assuming $\delta = 10$ ms and $T2 = 100$ ms.

In Vivo Measurements

Eight healthy volunteers (4 male) aged 25 to 55 years were recruited with approval from the ethics committee of University of Nottingham Medical School (Nottingham, UK) and participated in an experiment to 1) assess IVIM effects (a subgroup of 5 subjects participated; 3 male, aged 22–55 years), 2) measure $T2$, and 3) assess the diffusion time-dependent ADC in the brachial plexus. We repeated both experiments twice (three times for 1 volunteer) with a gap of at least 2 months to allow a qualitative assessment of reproducibility. MR Images of the brachial plexus were acquired using the cranial elements of the Torso XL 16 channel array coil, which was centered over the subject's thorax with padding used to prevent it touching the face.

The DWIBS scan consisted of a short tau inversion recovery images, fat-suppressed, multislice, single-shot echo planar imaging (EPI) readout with pulse gradient spin echo preparation. Axial/oblique scans were centered on the C5/C6 disc so that the imaged volume encompassed the C5 to T1 nerves in the cervical spine. The imaging parameters were field of view $192 \times 54 \times 300$ mm, 3-mm isotropic voxels, 18 slices with no gap, water/fat shift of 4.64 pixels, sense encoding (SENSE) factor = 2, EPI factor of 35, anterior-posterior fold-over direction, volume shimming with repetition time (TR) = 8,813 ms, and inversion time = 220 ms. The data acquisition was repeated to give two samples within each scanning session.

Initially to assess IVIM effects, subjects were scanned at $b = 0, 25, 50, 75, 100, 300, 500, 700,$ and 900 s/mm² with $TE = 60$ ms, $\Delta = 28.3$ ms, and $\delta = 10$ ms and a reference agar phantom placed above the subject's shoulder. A log-linear plot was used to identify the b value corresponding to reasonable separation between large-scale motion and diffusion. To measure $T2$, data were acquired for $TE = 55, 60, 65, 70, 75,$ and 80 ms with $b = 600$ s/mm², $\Delta = 28.3$ ms, $\delta = 10$ ms, and $TR = 6,000$ ms. $T2$ was calculated by weighted linear square fit to a monoexponential decay. Finally, to study the diffusion time dependence of ADC, data were acquired at $b = 300$ and 600 s/mm², $\Delta = 18.3, 25.3, 33.3, 41.3, 49.3, 57.3, 65.3, 73.3,$ and 81.3 ms, $\delta = 10$ ms, and $TE = 100$ ms. Data were also acquired from a phantom containing agar gel (4% [wt/wt] agar).

From a coronal MIP of the DWIBS data (Fig. 2a), two sagittal planes were selected through the multislice data set, orthogonal to the path of the nerves, on both sides of the body. Images of each plane were fitted to a multiple 2D Gaussian function (Fig. 2b), assuming that the nerve signal had an approximately Gaussian spatial profile, with the peak amplitudes providing an estimate of signal for each b value. The size of the nerve was of the order
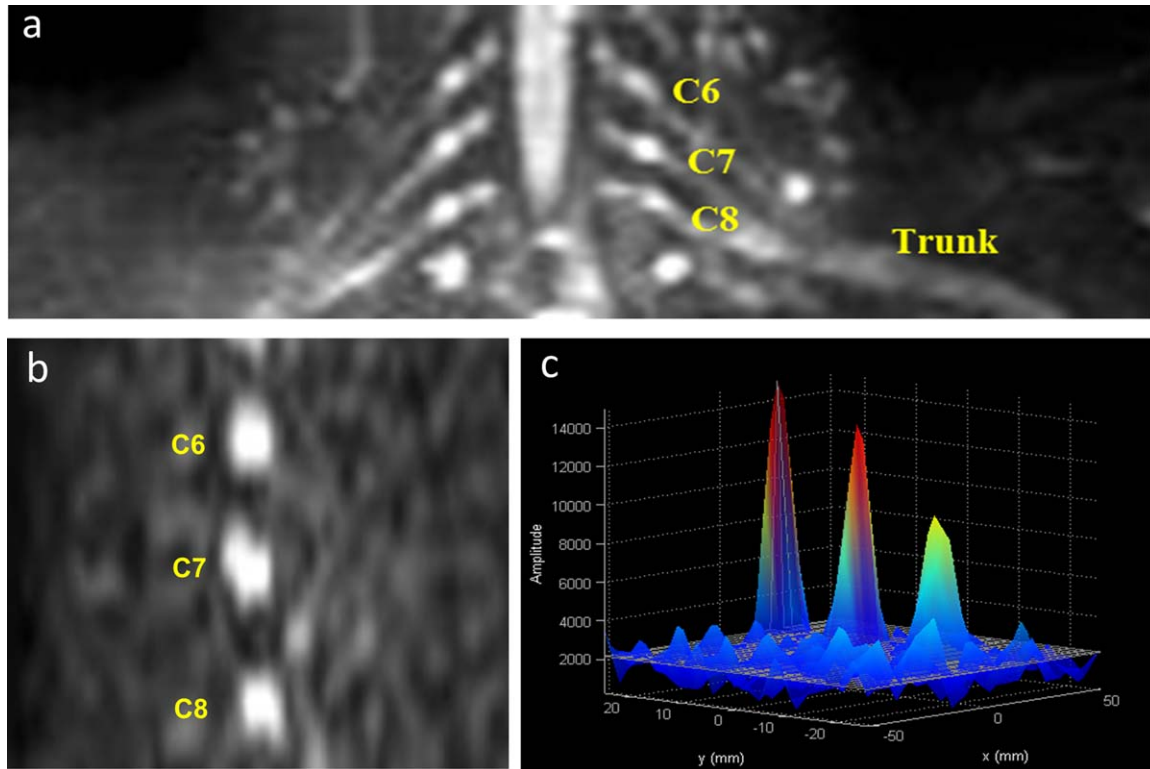
F2

FIG. 2. (**a**) Coronal view MIP of brachial plexus, obtained using DWIBS with b $=$ 300 s/mm^2. C6, C7, and C8 nerves are identified and used for positioning of sagittal view slices. (**b**) Sagittal view of brachial plexus showing locations of C6, C7, and C8 nerve roots at b $=$ 300 s/mm^2. (**c**) Corresponding 2D Gaussian fitting showing peak for each nerve.

of a voxel causing much of the signal to be partial volumed between voxels. This approach allowed us to quantify the signal taking account of signals distributed across a number of voxels, and empirically this function fitted the nerve signal profile well. Any peak less than twice the standard deviation of the locally assessed noise was neglected to avoid errors from Riccian noise, particularly in the IVIM analysis where low-signal data were acquired (32–34). The cord region of interest was selected on the raw transverse images, and a similar process was applied. This analysis was repeated for each acquisition separately and the results were averaged across the two samples and both sides of the neck. ADC values of nerves and cord were then calculated (Eq. [2]).

The variation of ADC with diffusion time was plotted and averaged over all visits for nerves and cord separately. The resulting data were fitted to Equation [1] for tortuosity (α) and surface-to-volume ratio (S/V) using the nonlinear least square fitting function in Matlab (The MathWorks, Inc., Natick, MA, USA). For this fit, the self-diffusion coefficient D_0 was derived by linear extrapolation of a plot of $D(\Delta)$ versus $\sqrt{\Delta}$ to $\Delta = 0$ and the time scaling factor θ estimated from the relation $\sqrt{D_0\theta} \sim$ neuron size as previously proposed (14,15).

RESULTS

F3   Figure 3 shows the simulated variations in the contrast to noise in diffusivity difference (Γ_K) with b value, for different ranges of Δ achievable at different echo times. Similar results were obtained by varying *T2* or restriction

size. The simulation also confirmed that short gradient lobes (small δ) and high b values maximized sensitivity to diffusion time. From these results, the difference
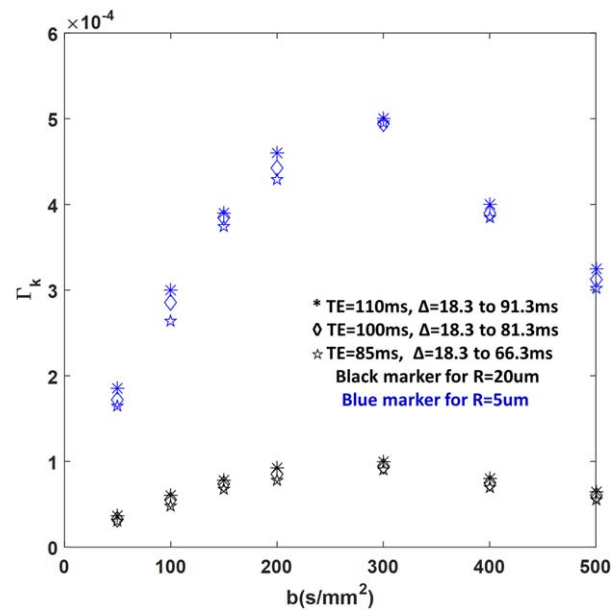
FIG. 3. Variation of contrast-to-noise ratio in the diffusion time dependence of the measured diffusion coefficient (Γ_K) with b-value at a range of Δ for different TE and $\delta = 10$ ms. ~~*TE$=$110 ms; $\diamond$TE$=$100 ms; *TE$=$85 ms; blue for R$=$20 µm, black for R$=$5 µm.~~
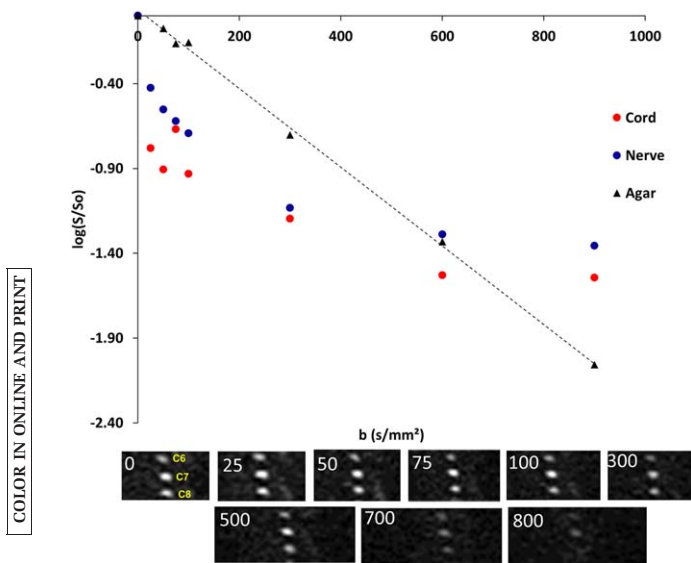
FIG. 4. Example IVIM plots for brachial plexus nerves, cord, and agar phantom. Agar phantom (black) shows a linear change with b-values because there is no IVIM effect. However, nerve (blue) and cord (red) signals show nonlinear behavior. Below the graph is shown a set of images from the IVIM data set showing the C6, C7, and C8 nerves for the range of b-values indicated on the figures (s/mm^2). ● Cord, ● Nerve, ▲ Agar.

between the high and low b value used experimentally was selected to be 300 s/mm^2.

F4   Figure 4 shows that the diffusion curve was approximately biexponential, with $b = 300$ s/mm^2 providing reasonable separation between IVIM and diffusion effects, and thus this value was selected as the low b value for subsequent measurements. The measured IVIM and T2

T2   parameters are shown in Table 2.

F5   Figures 5a shows the variation in ADC with Δ for 1 representative subject (the subject that was scanned three times), and Figure 5b shows the fit to the Latour-Mitra equation superimposed on the subject-averaged data. The average ADC was higher in the nerve than the cord at all values of diffusion time. Table 2 summarizes the results of fitting the data to the Latour-Mitra equation. No variation with diffusion time was observed for agar phantoms [ADC = $(1.5 \pm 0.008) \times 10^{-3}$ mm^2/s at room temperature].

DISCUSSION

This study detected restricted diffusion in the human brachial plexus in vivo using the DWIBS sequence on a clinical MRI scanner. Measured ADC values were in the

same range as previously reported in the nervous system (35). The larger ADC in the brachial plexus nerve than the cord is expected given that nerve fibers are larger.

There was a clear reduction in the ADC with increasing diffusion time for the nerves and cord, which was not observed in an agar phantom, suggesting that diffusion was restricted or hindered in these tissues. The longest accessible diffusion time, $\Delta_{max} = 81.3$ ms, corresponded to a mean diffusion length of $\sim 13\,\mu m$, which is similar to the diameter of the largest fibers in the brachial plexus nerves and cord, and the lack of an asymptote at high Δ indicates that diffusion was not fully restricted at the longest diffusion time, consistent with extra-axonal contributions. The short diffusion time, $\Delta_{min} = 18.3$ ms, probed a mean molecular displacement of around $8\,\mu m$, which corresponds to the diameters of the middle-range fibers, suggesting that sensitivity to observing smaller fibers could be achieved by using shorter diffusion times if larger gradients were available. The definition of diffusion time used here (Fig. 1) does not fully consider the effects of movement during the gradient pulses.

The measured $T2$ values were comparable with previous results (36). The longer values recorded in the cord and the greater intra-subject variation may indicate cerebrospinal fluid contributions or motion artefacts. It was also found that IVIM-type effects contributed to signals from the nerves and cord collected at $b < \sim 300$ s/mm^2. This was assessed for $\Delta = 28.3$ ms and it would be interesting to investigate how these effects vary with diffusion time. The b value used for diffusion time-dependent measurements was optimized to maximize the sensitivity to a change in measured diffusion coefficient with diffusion time (Γ_K), for accessible scanner timing parameters, based on a simple Monte Carlo simulation of restricted diffusion within a simplified model. Γ_K decreased at short TE over the range considered because the accessible range of Δ was small. Γ_K decreased at high b value because the SNR in the measured value of D fell, and decreased at low b value because the absolute variation in D with Δ was small, giving a maximum in Γ_K at b ~ 300 s/mm^2. In practice, the low b value used in vivo (b_1) needed to be 300 s/mm^2 to eliminate IVIM-type effects; therefore, given that the accessible range of diffusion time was similar across a wide range of b values (Table 1), the high b value used in vivo (b_2) was 600 s/mm^2.

The diffusion time dependency of the ADC data was fitted to the Latour-Mitra porous media model. The measured values of α and S/V were in the range previously obtained for other biological samples such as red blood

Table 2
Measured Values of *T2*, IVIM Parameters, and the Latour-Mitra Equation Fitting Parameters and α and *S/V* (Intersubject Mean and Standard Deviation).

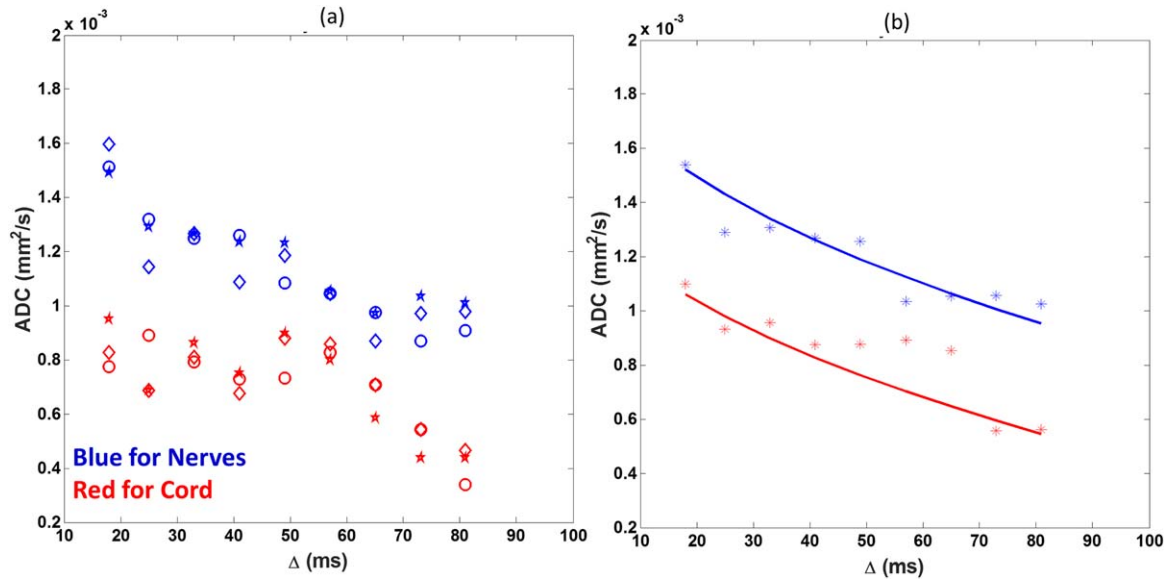|		IVIM Results Measured for $\Delta = 28.3$ ms			Latour-Mitra Equation Fit			
Region	T2 (ms)	f	D* ($\times 10^{-3}$ mm^2/s)	D ($\times 10^{-3}$ mm^2/s)	D$_0$ ($\times 10^{-3}$ mm^2/s)	θ ($\times 10^{-2}$ s)	α	S/V (mm^{-1})
Nerve	80 ± 5	0.24 ± 0.01	10 ± 7	1.1 ± 0.02	1.898 ± 0.005	5.26 ± 0.5	6.9 ± 0.1	132 ± 7
Cord	100 ± 6	0.48 ± 0.02	70 ± 7	0.9 ± 0.01	1.527 ± 0.005	6.66 ± 0.2	4.3 ± 0.3	260 ± 20

Mahbub et al.

FIG. 5. Measured variation in ADC with Δ for nerves and cord of the brachial plexus for (**a**) subject 1 with each repeat of the measurement being indicated by a different marker. (**b**) Data averaged over repeated measurements for 8 subjects, with fit to the Latour equation superimposed. ✳ Cord Data, ✳ Nerve Data, ▬ Cord Data fit ▬ Nerve Data fit.

cells and cerebral tumors (8,15). S/V and α relate to the characteristic sizes of the structures restricting or hindering the diffusion, so the smaller values of S/V in the nerve would be expected given that the fibers are larger with consequently larger interfiber spaces than in the cord, and the larger values of α found in the nerves indicate greater hindrance to movement of water molecules than in the cord. However, the tortuosity α cannot be estimated reliably unless a high-diffusion time asymptote is reached, which was not detected in the cord and was not clearly detected in the nerve in this work. The Latour model is inherently a 3D model, but, in this case, we were applying it to a system that is restricted in only two dimensions and were only encoding diffusion in one direction, which was not exactly perpendicular to the nerve fibers. This will alter the physical interpretation of the fitted parameters and also make them dependent on the exact orientation of the diffusion gradients relative to the nerve fibers. This could be overcome in the future by ensuring that diffusion is measured in an anatomically consistent direction.

Future work should focus on measuring this parameter in a range of nervous tissue and should consider other restricted diffusion models. Assessment of microstructure in the peripheral nerves has potential in monitoring inflammatory neuropathies, and so future work should also investigate whether diffusion time-dependent ADC provides additional clinical information, and, if so, the optimum diffusion time would provide sensitivity to changes in disease.

CONCLUSION

We have developed a novel method of probing restricted and hindered diffusion in the brachial plexus nerves and cord. The porous media, time-dependent diffusion model was used to characterize restricted diffusion in these tissues. Resulting estimates of the surface to volume ratio

and tortuosity were comparable with values obtained previously on biological systems and can give information about the intra-axonal and extra-axonal spaces.

REFERENCES

1. Bonnel F. Microscopic anatomy of the adult human brachial plexus: an anatomical and histological basis for microsurgery. Microsurgery 1984;5:107–117.
2. Sunderland S, Bradley K. The cross-sectional area of peripheral nerve trunks devoted to nerve fibres. Brain 1949;72:428–449.
3. Le Bihan D, Delannoy J, Levin RL. Temperature mapping with MR imaging of molecular diffusion: application to hyperthermia. Radiology 1989;171:853–857.
4. Assaf Y, Basser PJ. Composite hindered and restricted model of diffusion (CHARMED) MR imaging of the human brain. NeuroImage 2005;27:48–58.
5. Assaf Y, Blumenfeld-Katzir T, Yovel Y, Basser PJ. AxCaliber: a method for measuring axon diameter distribution from diffusion MRI. Magn Reson Med 2008;59:1347–1354.
6. Le Bihan D. Molecular diffusion, tissue microdynamics and microstructure. NMR Biomed 1995;8:375–386.
7. Novikov DS, Fieremans E, Jensen JH, Helpern JA. Random walks with barriers. Nat Phys 2011;7:508–514.
8. Latour LL, Svoboda K, Mitra PP, Sotak CH. Time-dependent diffusion of water in a biological model system. Proc Natl Acad Sci U S A 1994;91:1229–1233.
9. Sigmund EE. Perspectives on porous media MR in clinical MRI. AIP Conf Proc 2011;1330:13–16.
10. Mitra PP. Diffusion in porous materials as probed by pulsed gradient NMR measurements. Physica A 1997;241:122–127.
11. Mitra PP, Sen PN, Schwartz LM. Short-time behavior of the diffusion coefficient as a geometrical probe of porous media. Phys Rev B Condens Matter 1993;47:8565–8574.
12. Mitra PP, Sen PN, Schwartz LM, Le Doussal P. Diffusion propagator as a probe of the structure of porous media. Phys Rev Lett 1992;68:3555–3558.
13. Sen PN. Time-dependent diffusion coefficient as a probe of geometry. Concepts Magn Reson Part A 2004;23A:1–21.
14. Latour LL, Mitra PP, Kleinberg RL, Sotak CH. Time-dependent diffusion coefficient of fluids in porous media as a probe of surface-to-volume ratio. J Magn Reson 1993;101:342–346.
15. Helmer KG, Dardzinski BJ, Sotak CH. The application of porous-media theory to the investigation of time-dependent diffusion in in vivo systems. NMR Biomed 1995;8:297–306.

16. Zhao L, Sukstanskii AL, Kroenke CD, Song J, Piwnica-Worms D, Ackerman JJ, Neil JJ. Intracellular water specific MR of microbead-adherent cells: HeLa cell intracellular water diffusion. Magn Reson Med 2008;59:79–84.

17. Ghosh PK, Jayas DS, Gruwel ML. Measurement of water diffusivities in barley components using diffusion weighted imaging and validation with a drying model. Dry Technol 2009;27:382–392.

18. Fieremans E, De Deene Y, Delputte S, Ozdemir MS, D'Asseler Y, Vlassenbroeck J, Deblaere K, Achten E, Lemahieu I. Simulation and experimental verification of the diffusion in an anisotropic fiber phantom. J Magn Reson 2008;190:189–199.

19. Parsons EC, Does MD, Gore JC. Temporal diffusion spectroscopy: theory and implementation in restricted systems using oscillating gradients. Magn Reson Med 2006;55:75–84.

20. Takahara T, Imai Y, Yamashita T, Yasuda S, Nasu S, Van Cauteren M. Diffusion weighted whole body imaging with background body signal suppression (DWIBS): technical improvement using free breathing, STIR and high resolution 3D display. Radiat Med 2004;22: 275–282.

21. Mürtz P, Krautmacher C, Träber F, Gieseke J, Schild H, Willinek W. Diffusion-weighted whole-body MR imaging with background body signal suppression: a feasibility study at 3.0 Tesla. Eur Radiol 2007; 17:3031–3037.

22. Takahara T, Hendrikse J, Yamashita T, Mali WP, Kwee TC, Imai Y, Luijten PR. Diffusion-weighted MR Neurography of the brachial plexus: feasibility study. Radiology 2008;249:653–660.

23. Vargas MI, Viallon M, Nguyen D, Beaulieu JY, Delavelle J, Becker M. New approaches in imaging of the brachial plexus. Eur J Radiol 2010; 74:403–410.

24. Yamashita T, Kwee TC, Takahara T. Whole-body magnetic resonance neurography. N Engl J Med 2009;361:538–539.

25. Mürtz P, Kaschner M, Lakghomi A, Gieseke J, Willinek WA, Schild HH, Thomas D. Diffusion-weighted MR neurography of the brachial

26. Takahara T, Kwee TC. MR Neurography: Imaging of the Peripheral Nerves. Diffusion-Weighted MR Imaging. Berlin; Heidelberg, Germany: Springer-Verlag; 2010:51–67.

27. Z B Mahbub PG. IVIM, T2 and Time Dependent Diffusivity study of Nerve and Spinal cord. In Proceedings of the 29th Annual Scientific Meeting of ESMRMB, Lisbon, Portugal, 2012. p. ePoster-56.

28. Z B Mahbub PG. Measurement of magnetization transfer effects in the brachial plexus: comparison with T2 and Diffusion effects. In Proceedings of the 21st Annual Meeting & Exhibition of ISMRM, Salt Lake City, UT, USA 2013. p. 1219.

29. Conturo TE, McKinstry RC, Aronovitz JA, Neil JJ. Diffusion MRI: precision, accuracy and flow effects. NMR in Biomedicine 2005;8(7):307–332.

30. Jones DK. Optimal approaches to diffusion MRI acquisition. In Jones DK, ed. Diffusion MRI: Theory, Methods, and Applications. Oxford, UK; New York: Oxford University Press; 2010:250–271.

31. Bito Y, Hirata S, Yamamoto E. Optimum gradient factors for apparent diffusion coefficient measurements. In Proceedings of the Annual Joint Meeting of SMR/ESMRMB, Nice, France, 1995. p. 913.

32. Henkelman RM. Measurement of signal intensities in the presence of noise in MR images. Med Phys 1985;12:232–233.

33. Macovski A. Noise in MRI. Magn Reson Med 1996;36:494–497.

34. Aja-Fernández S, Vegas-Sánchez-Ferrero G, Tristán-Vega A. Noise estimation in parallel MRI: GRAPPA and SENSE. Magn Reson Imaging 2014;32:281–290.

35. Rangwala NA, Hackney DB, Dai WY, Alsop DC. Diffusion restriction in the human spinal cord characterized in vivo with high b-value STEAM diffusion imaging. Neuroimage 2013;82:416–425.

36. MacMillan EL, Mädler B, Fichtner N, Dvorak MF, Li DK, Curt A, MacKay AL. Myelin water and T2 relaxation measurements in the healthy cervical spinal cord at 3.0T: repeatability and changes with age. NeuroImage 2011;54:1083–1090.

AQ4

AQ1: For title, a hyphen has been added for "Time-Dependent" as in text when used adjectively; please approve change as OK.

AQ2: Author first names have been copied in from a separate editorial file. Please confirm that all author names are appearing correctly

AQ3: Please confirm city for author affiliation 1 as correct.

AQ4: For references 27 and 28, please provide full details for list of authors.

AQ5: If desired, please provide corresponding author's Twitter handle. Also, if applicable, please provide complete postal address along with street name and number or post office box. Please also provide for corresponding author highest academic degree(s) attained.

AQ6: Please confirm that given names (red) and surnames/family names (green) have been identified correctly